Probing the density dependence of the symmetry potential at low and high densities

Qingfeng Li [1*] , Zhuxia Li [1,2] , Sven Soff [3], Marcus Bleicher [3], and Horst Stöcker [1,3]

1) Frankfurt Institute for Advanced Studies (FIAS),

Johann Wolfgang Goethe-Universität,

Max-von-Laue-Str. 1,

D-60438 Frankfurt am Main, Germany

2) China Institute of Atomic Energy,

P.O. Box 275 (18),

Beijing 102413, P.R. China

3) Institut für Theoretische Physik,

Johann Wolfgang Goethe-Universität,

Max-von-Laue-Str. 1,

D-60438 Frankfurt am Main, Germany

Abstract

We investigate the sensitivity of several observables to the density dependence of the symmetry potential within the microscopic transport model UrQMD (ultrarelativistic quantum molecular dynamics model). The same systems are used to probe the symmetry potential at both low and high densities. The influence of the symmetry potentials on the yields of π^-, π^+, the π^-/π^+ ratio, the n/p ratio of free nucleons and the $t/^3$He ratio are studied for neutron-rich heavy ion collisions ($^{208}Pb+^{208}Pb$, $^{132}Sn+^{124}Sn$, $^{96}Zr+^{96}Zr$) at $E_b = 0.4A$ GeV. We find that these multiple probes provides comprehensive information on the density dependence of the symmetry potential.

PACS numbers: 24.10.Lx, 25.75.Dw, 25.75.-q

* Fellow of the Alexander von Humboldt Foundation.

The nuclear equation of state (EoS) for isospin-asymmetric nuclear systems has recently attracted a lot of attention. The EoS for isospin-asymmetric nuclear matter can be described approximately by the parabolic law (see, e.g., [1])

$$e(\rho,\delta) = e_0(\rho,0) + e_{\rm sym}(\rho)\delta^2, \tag{1}$$

where $\delta = (\rho_n - \rho_p)/(\rho_n + \rho_p)$ is the isospin asymmetry defined by the neutron (ρ_n) and proton (ρ_p) densities. e_0 is the energy per nucleon for symmetric nuclear matter and $e_{\rm sym}(\rho)$ is the bulk symmetry energy. The nuclear symmetry energy term $e_{\rm sym}(\rho)$ is very important for the understanding of many interesting astrophysical phenomena, but it is also plagued by large uncertainties. An extreme variation of the EoS is observed for neutron-rich matter by using different versions of the Skyrme interaction as well as other non-relativistic effective interactions [2]. The EoS of neutron-rich matter can be studied using a density-dependent relativistic hadron mean-field theory like the DDH3$\rho\delta$ and DDHρ models [3]. The density dependence of the symmetry potential deduced from relativistic and non-relativistic interactions might be different. Therefore, a comparison of the isospin effect in isospin-asymmetric heavy ion collisions (HICs) with both relativistic and non-relativistic effective interactions is important. Furthermore, most of the studies on sensitive probes of the density dependence of the symmetry potential are concerned with the behavior in the low-density or in the high-density region separately. Thus the simultaneous study of observables, which are sensitive to both the low-density and the high-density part of symmetry potential, in one reaction system is necessary. This allows to extract the full information on the density dependence of the symmetry potential which relates to specific effective interactions.

To study the isospin effects in intermediate energy HICs, heavy stable nuclei with an isospin asymmetry as large as possible should be used. They have the advantage that both, the availability and the beam intensities are much higher than for radioactive beams and, hence, high statistics experimental data can be obtained. This is necessary to study the relatively subtle effects of different symmetry potentials. The reaction $^{208}Pb + ^{208}Pb$, for example, has an isospin-asymmetry $\delta \simeq 0.212$, i.e., a neutron to proton ratio $N/Z \simeq 1.54$, which is already quite large [4].

In a previous work, we have adopted the following forms of the symmetry potential [5]

$$F(u) = \begin{cases} F_1 = u^\gamma \ , & \text{with} \quad \gamma > 0 \\ F_2 = u \cdot \frac{a-u}{a-1} \ , & \text{with} \quad a > 1 \end{cases} , \tag{2}$$

to mimic the strong variation of the density dependence of the symmetry potential at high densities as given by the Skyrme-type interactions. Here, $u = \rho/\rho_0$ is the reduced density and a is the reduced critical density. When $u > a$, the symmetry potential energy is negative in F_2. We choose $\gamma = 1.5$ ($a = 3$) for F_1 (F_2) and name it F15 (Fa3). In the present work we further adopt two other forms of the symmetry potential based on the relativistic mean field theory, namely DDH3$\rho\delta^*$ and DDHρ^*. Both are based on the extended QHD model (see Ref. [3]). The density dependence of the symmetry potentials for the DDH3$\rho\delta$ and DDHρ models is due to the density dependence of the coupling constants ($g_{\sigma N}$, $g_{\omega N}$, $g_{\rho N}$, and $g_{\delta N}$). Fig. 1 shows the density dependences of these symmetry potentials as well as the linear case. For comparison, we fix the symmetry potential energy at normal nuclear density for all four forms of the symmetry potential. The symmetry energy coefficient is adopted to be $S_0 = 34$ MeV [6, 7]. It is seen from Fig. 1 that, for $u < 1$, DDH3$\rho\delta^*$ is very close to Fa3, both of them lie between DDHρ^* and F15. For $u > 1$, they show a rather different behavior and approach F15 and DDHρ^*, respectively.

In the present work, central collisions are studied for the three neutron-rich systems $^{208}Pb + ^{208}Pb$ ($\delta \simeq 0.212$), $^{132}Sn + ^{124}Sn$ ($\delta \simeq 0.218$), and $^{96}Zr + ^{96}Zr$ ($\delta \simeq 0.167$) at $E_b = 0.4A$ GeV. The ultrarelativistic quantum molecular dynamics model (UrQMD, version 1.3) [8, 9, 10, 11] is adopted for the calculations including the Coulomb potential for charged pions. A 'hard' Skyrme-type EoS ($K = 300$ MeV) without momentum dependence is used for the calculations. It should be noted that the uncertainty of the isospin independent EoS is still large (see Refs. [6, 12]), and the contribution of the momentum dependence in EoS is also important to the dynamics of HICs (see Ref. [13]), both of them influence the results but do not change the effect of the density dependence of symmetry potential on the ratios of different charged particles strongly [14].

Figs. 2 and 3 show the rapidity and the transverse momentum distributions of π^- and π^+ for central ($b = 0 - 2$ fm) $^{208}Pb + ^{208}Pb$ collisions at $0.4A$ GeV as calculated with the symmetry potentials $F15$ and $Fa3$. Fig. 3 also shows the corresponding π^-/π^+ ratios. While the π^- yields are quite sensitive to the symmetry potential at mid-rapidity and at low $p_t^{\rm cm}$, the π^+ do not exhibit this sensitivity due to the neutron-rich environment [14]. The calculations for the $^{132}Sn + ^{124}Sn$ and $^{96}Zr + ^{96}Zr$ reactions are similar to those in Figs. 2 and 3. To analyze the differences in the π^- and π^+ yields and the π^-/π^+ ratios (as calculated with the four different forms of the symmetry potential) more quantitatively, we

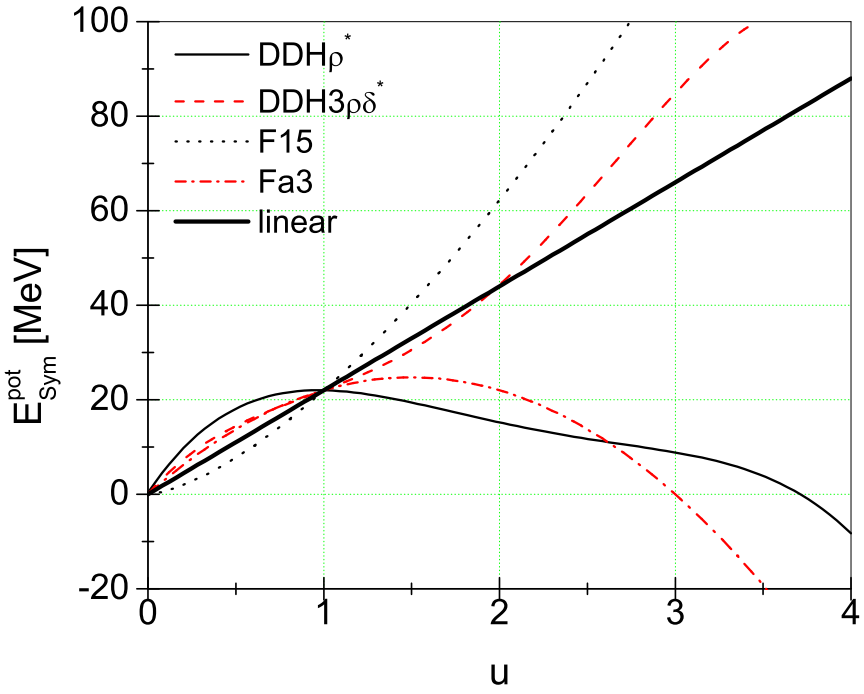

FIG. 1: Parametrizations of the nuclear symmetry potential DDHρ^*, DDH3$\rho\delta^*$, F15, Fa3, and the linear one as a function of the reduced density u.

define a variable $D_{ij} = (X_i - X_j)/X_j$, where the subscripts "i" and "j" denote different forms of the symmetry potential. "X" represents the calculated quantity, such as the pion yield or the π^-/π^+ ratio. Here, i denotes the symmetry potential that yields a larger X value than the one with the symmetry potential j, i.e., we always choose $X_i > X_j$. Table I (for $^{208}Pb + ^{208}Pb$, titled as "$Pb208$") and Table II (for $^{132}Sn + ^{124}Sn$, titled as "$Sn132$") give the results of D_{ij} for different conditions and physical cuts: the subscript "tot" indicates the results without any kinematical cut, "$y \sim 0$" denotes particles emitted at mid-rapidity (y_c in the center-of-mass system), and the subscript "$p_t \sim 0.1$" means the particles with transverse momenta $p_t^{\rm cm} \simeq 0.1A\,{\rm GeV}/c$. Here, the index 1 represents the "DDH3$\rho\delta^*$" symmetry potential, 2 represents "DDHρ^*", 3 represents "F15", and 4 is the "Fa3" case. D_{max} provides the maximum value of all D_{ij}. The differences are maximal for the D_{23} values, these are the differences between the F15 and DDHρ^* symmetry potentials, which

also exhibit the largest deviations in the density dependence of the symmetry potential at densities $u \sim 1 - 2.6$ (see Fig. 1). Tables I and II demonstrate that the values of D_{ij} for π^+ are always smaller than those for π^-, this is consistent with Figs. 2 and 3. By comparison, we find that the π^-/π^+ ratio at $p_t^{\rm cm} \simeq 0.1\,{\rm GeV}/c$ is most suitable to probe the symmetry potential because of the larger π^- and π^+ yields in this transverse momentum region. We divide all D_{ij} into two groups in Tables I and II. In general, the values in the first group of D_{21}, D_{43} and $D_{max}(= D_{23})$ are much larger than those in the second group of D_{13}, D_{41}, D_{24}. For the former case the values are generally larger or close to 10 except for the π^+, while for the latter one they are all smaller than 10, except D_{13} for the π^-/π^+ ratio at $p_t^{\rm cm} \simeq 0.1\,{\rm GeV}/c$ with a value of 10. Surprisingly, D_{41} lies in the second group, although Fa3 corresponds to a soft symmetry potential and DDH3$\rho\delta^*$ corresponds to a stiff symmetry potential. The reason can be found in Fig. 1: the difference between these two symmetry potentials is not large for reduced densities $u = 1 \sim 2$ where most of the pions are produced [15]. It means that more accurate measurements are needed in order to probe the density dependence of the symmetry potential with pions, except for the extreme cases. Furthermore, from Tables I and II we observe $X_{DDH\rho^*} > X_{Fa3} > X_{DDH3\rho\delta^*} > X_{F15}$. This order agrees with the order of the four forms of the symmetry potentials at baryon densities $u \simeq 1 - 2$ (see Fig. 1). Baryon densities of $u \simeq 1 - 2$ are the most relevant ones for pion production as we have shown in [5, 15]. Comparing the values D_{ij} shown in Tables I and II, we see that the values D_{ij} are a little smaller for $^{208}Pb + ^{208}Pb$ as compared to $^{132}Sn + ^{124}Sn$ with radioactive beams.

Probes being sensitive to the density dependence of the symmetry potential at subnormal densities have been studied extensively in recent years. Usually a form $(\rho/\rho_0)^\gamma$ is assumed for the density dependence of the symmetry potential [16]. From Fig. 1 it follows that the behavior of the symmetry potential at subnormal and high densities are quite different. To gain information on the symmetry potential in both, the high and the subnormal density regions simultaneously, observables from the same reaction system are needed, which are sensitive to both density regions. Most of the free nucleons, intermediate mass fragments and light charged particles are emitted in the expansion stage, that is, at subnormal densities. Therefore, we further study the ratios of free neutrons and protons, the isotope distributions of light and intermediate mass fragments, as well as the ratio of emitted tritons and ^{3}He which is also proposed as a sensitive probe for the symmetry potential at subnormal densities

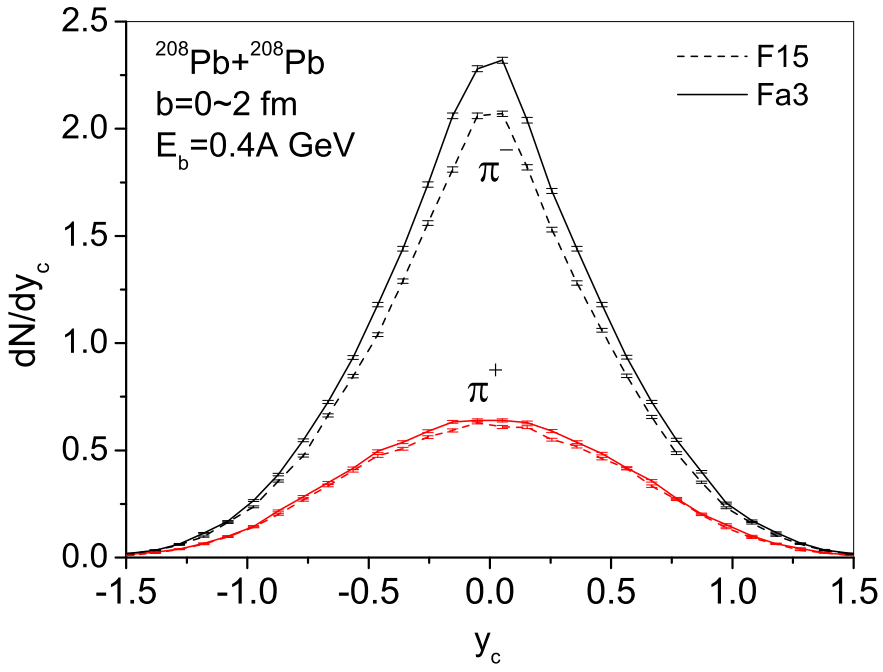

FIG. 2: The rapidity distributions of π^- and π^+ for central $^{208}Pb+^{208}Pb$ collisions with different symmetry potentials (see text).

[17]. A conventional phase-space coalescence model [18] is used to construct the clusters, in which the nucleons with relative momenta smaller than P_0 and relative distances smaller than R_0 are considered to belong to one cluster. In this work P_0 and R_0 are chosen to be $0.3\,\mathrm{GeV}/c$ and 3.5 fm, respectively. Another set, $P_0 = 0.25\,\mathrm{GeV}/c$ and $R_0 = 3.0$ fm, alters the yields of free nucleons and clusters strongly, but it does not change the dependence of the $t/^3$He ratios on the symmetry potentials. The freeze-out time is taken to be 150 fm/c. In Ref. [17] a modified coalescence model [19] was adopted. It was found that a modification of the coalescence criteria changes the yields of light charged particles but it does not change the $t/^3$He ratio.

Fig. 4 shows the transverse momentum distribution of the n/p ratios of emitted unbound nucleons as calculated with the four different forms of the symmetry potential. The n/p ratio obviously depends strongly on the choice of the symmetry potential. In the low transverse momentum region the n/p ratio is the largest for DDHρ^* and the smallest for F15. Obviously, nucleons with low transverse momenta are mainly emitted from the low density region.

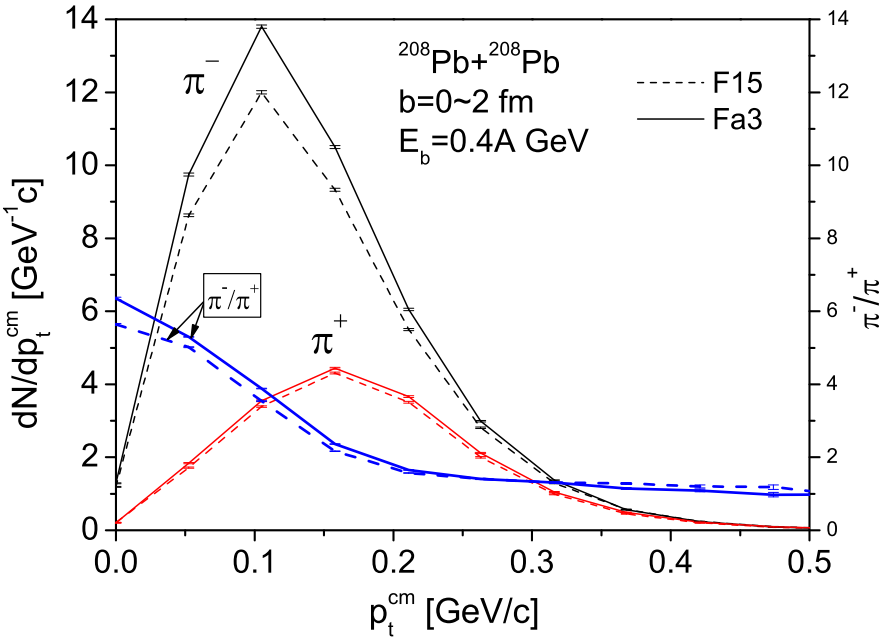

FIG. 3: Transverse momentum distributions of π^- and π^+ from central $^{208}Pb+^{208}Pb$ collisions at $E_b = 0.4A\,\mathrm{GeV}$ for different symmetry potentials. The π^-/π^+ ratios are also shown as a function of transverse momentum.

TABLE I: Values D_{ij} of the total $\pi^\pm$ yields (at mid-rapidity or $p_t^{\rm cm} \simeq 0.1\,\mathrm{GeV}/c$) and of the corresponding π^-/π^+ ratios for various combinations of the density-dependent symmetry potentials for $^{208}Pb+^{208}Pb$ reactions (see text).

"Pb208"	π^-_{tot}	$\pi^-_{y\sim0}$	$\pi^-_{p_t\sim0.1}$	π^+_{tot}	$\pi^+_{y\sim0}$	$\pi^+_{p_t\sim0.1}$	$(\frac{\pi^-}{\pi^+})_{tot}$	$(\frac{\pi^-}{\pi^+})_{y\sim0}$	$(\frac{\pi^-}{\pi^+})_{p_t\sim0.1}$
D_{21} [%]	14	13	16	9	11	9	5	2	6
D_{43} [%]	12	11	15	5	3	5	7	8	10
D_{max} [%]	20	18	24	10	12	9	8	5	18
D_{13} [%]	5	5	7	1	1	0	4	3	10
D_{41} [%]	6	6	8	4	2	5	3	4	0
D_{24} [%]	7	6	8	5	8	4	2	5	7

TABLE II: The same as in Table I but for $^{132}Sn + ^{124}Sn$ reactions.

"Sn132"	π^-_{tot}	$\pi^-_{y\sim0}$	$\pi^-_{p_t\sim0.1}$	π^+_{tot}	$\pi^+_{y\sim0}$	$\pi^+_{p_t\sim0.1}$	$(\frac{\pi^-}{\pi^+})_{tot}$	$(\frac{\pi^-}{\pi^+})_{y\sim0}$	$(\frac{\pi^-}{\pi^+})_{p_t\sim0.1}$
D_{21} [%]	12	11	13	5	6	6	6	5	7
D_{43} [%]	11	10	13	4	4	3	7	6	10
D_{max} [%]	19	17	21	7	8	6	11	9	18
D_{13} [%]	6	5	7	1	2	0	5	3	10
D_{41} [%]	5	5	6	3	2	4	2	3	0
D_{24} [%]	6	6	7	2	3	2	4	2	8

From Fig. 1 it follows that the difference between Fa3 and DDH3$\rho\delta^*$ is small at densities $\rho < \rho_0$. Correspondingly, the n/p ratios calculated with Fa3 and DDH3$\rho\delta^*$ are also very close at lower transverse momenta. For emitted nucleons with transverse momenta larger than ~ 700 MeV/c, the n/p ratios in the Fa3 and DDH3$\rho\delta^*$ cases are close to those in the DDHρ^* and F15 cases, respectively. This reflects the fact that $E^{\rm pot}_{\rm sym}$ for Fa3 (DDH3$\rho\delta^*$) is close to DDHρ^* (F15) when $\rho > \rho_0$. Free nucleons with transverse momenta larger than $\sim\ 700 MeV/c$ are mainly squeezed out from higher densities [20]. Thus, the different behavior of the n/p ratio as a function of *transverse momentum* goes in line with the behavior of the symmetry potential at low and high *densities* as shown in Fig. 1. The relative difference between the n/p ratios for transverse momenta larger than ~ 700 MeV/c as calculated with the soft and stiff symmetry potentials is on the same order as for the π^-/π^+ ratios.

To see the different emission times for nucleons with high and low transverse momenta, Fig. 5 shows the transverse momentum distributions of free neutrons and protons (upper plot) as well as the corresponding n/p ratios (lower plot), emitted from the mid-rapidity region ($|(y^{(0)}_c| = |y_c/y_{beam}| < 0.3$) at reaction times $t = 50$ and 150 fm/c. In the upper plot of Fig. 5 only the results for F15 are shown while the ratios for both the F15 and DDHρ^* symmetry potentials are compared in the lower plot. Nucleons with large transverse momenta are emitted in the early stage of the reaction and nucleons with small transverse momenta are emitted at later time. Furthermore, we see an obvious change of the transverse momentum distribution of the n/p ratios with time, especially in the low transverse momentum region, in particular in the case of the soft symmetry potential DDHρ^*. This can easily be understood from Fig. 1: in the cases of the soft symmetry potentials $DDH\rho^*$ and Fa3,

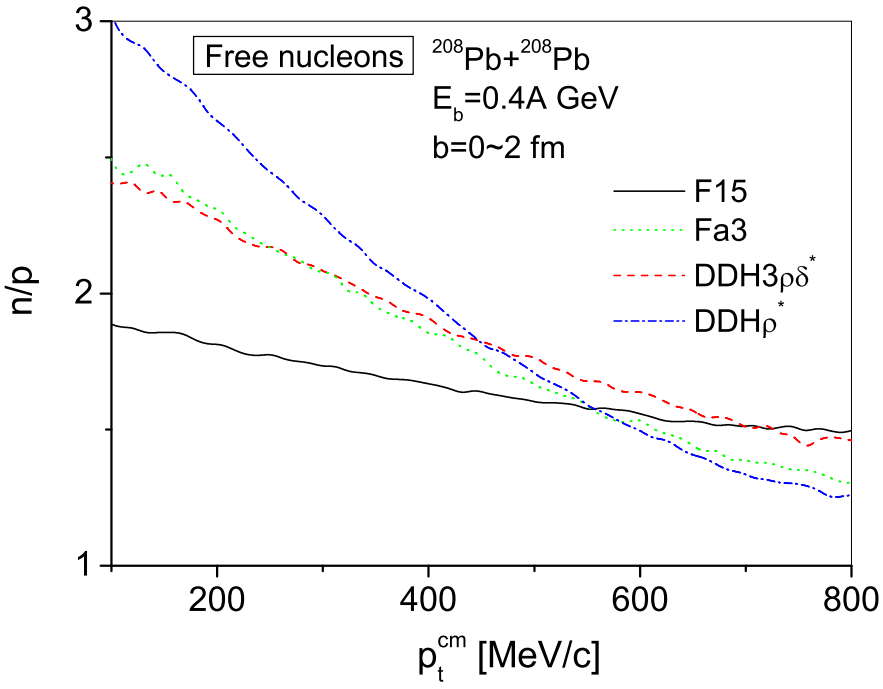

FIG. 4: Transverse momentum distributions of free neutron/proton ratios for different density-dependent symmetry potentials.

neutrons are strongly attracted into the high density region by the symmetry potential at the compression stage. Within the expansion period, neutrons are driven to lower densities, eventually leading to the subnormal densities. At subnormal densities the soft symmetry potential energy is higher than the stiff one. Hence, more neutrons with lower transverse momenta are emitted for the cases with soft symmetry potentials $DDH\rho^*$ and Fa3 at the later stage (at 150 fm/c) as compared to the cases with the stiff symmetry potentials. For the stiff symmetry potential case, there is no significant change of the transverse momentum distributions of the n/p ratio from t = 50 fm/c to 150 fm/c. In the high transverse momentum region, the n/p ratios for both cases decrease with time during the expansion phase, which happens mainly due to the extra Coulomb effect on the protons.

However, experimentally it is difficult to measure the spectra of neutrons with high precision. Therefore, the production of light charged particles with large but different N/Z ratios as well as isotope distributions for some intermediate mass fragments could be more useful [21, 22]. Fig. 6 shows the isotope distributions of $^{1-3}$H, $^{3-6}$He, $^{6-8}$Li, $^{8-11}$Be, $^{10-13}$B

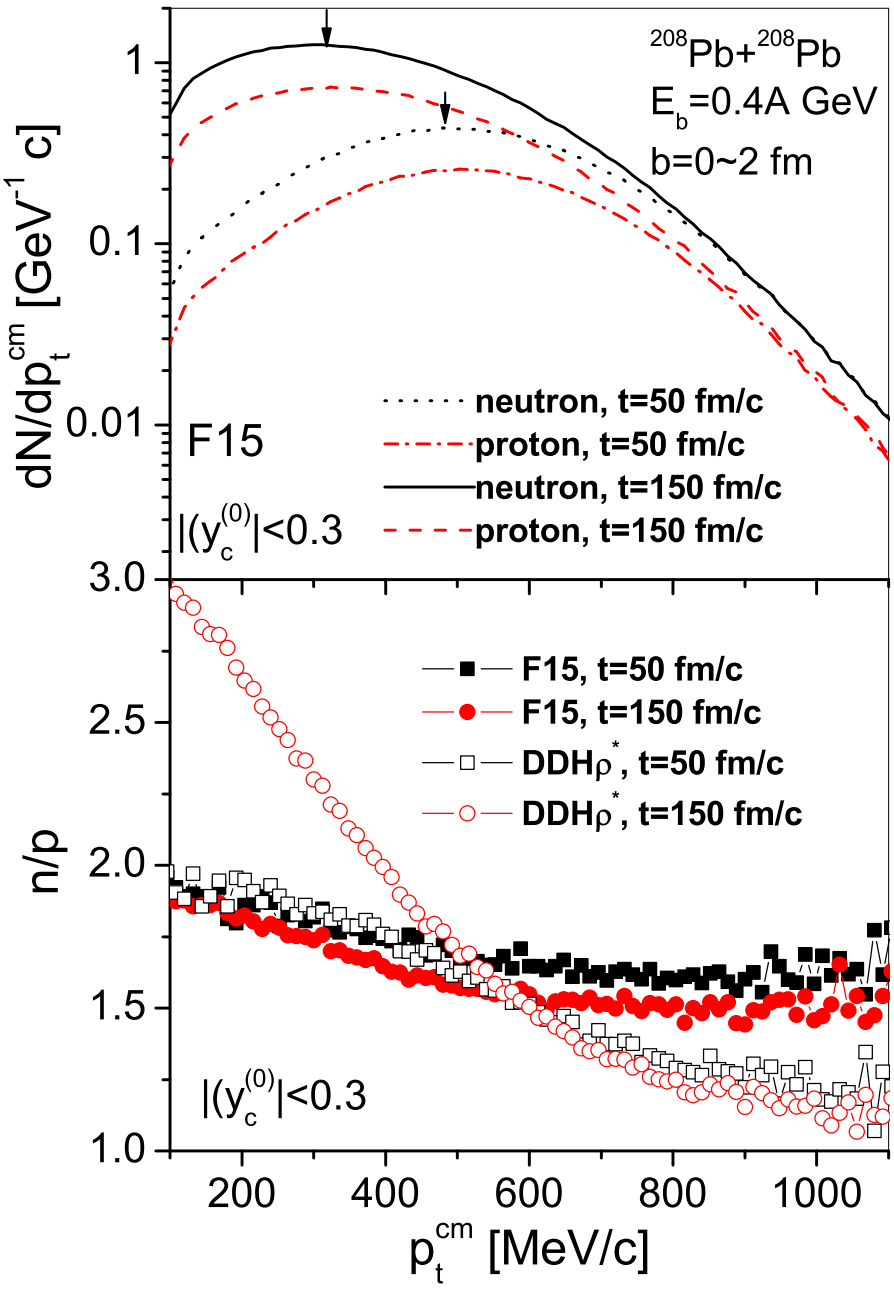

FIG. 5: Transverse momentum distributions of free neutrons and protons (upper plot) as well as the corresponding n/p ratios (lower plot) at mid-rapidity ($|(y_c^{(0)}| < 0.3$) and at reaction times t = 50 and 150 fm/c. The F15 and DDHρ^* symmetry potentials are chosen. The arrows in the upper plot show the maxima of the distributions.

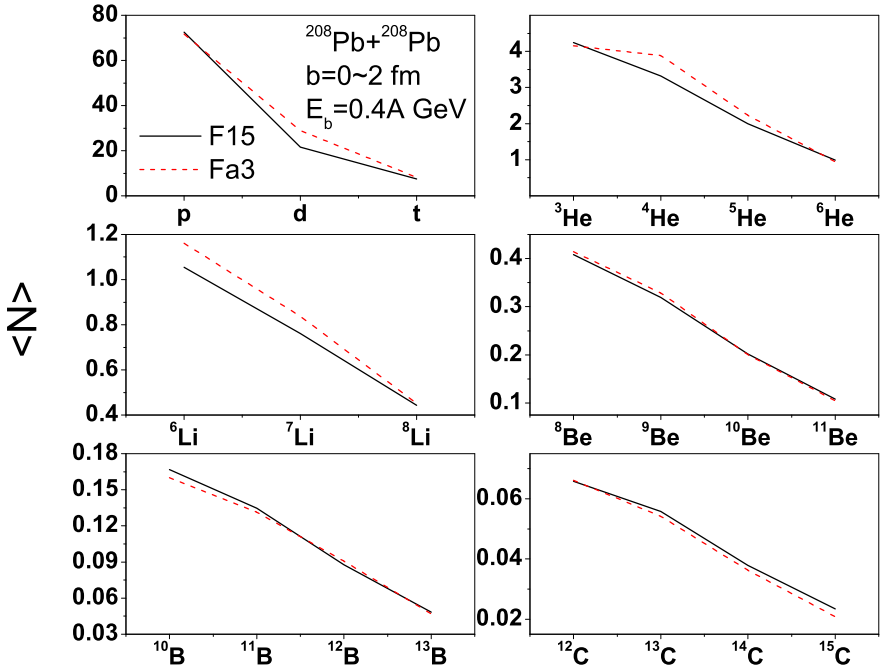

FIG. 6: Isotope distributions of H, He, Li, Be, B and C with the symmetry potentials F15 and Fa3 (see text).

and $^{12-15}$C in central Pb+Pb collisions as calculated with the symmetry potentials F15 and Fa3, respectively. In general, the differences between the isotope yields for the F15 and Fa3 cases are smaller than the differences in the n/p ratio of emitted nucleons. However, as the isotopes become more neutron-rich, the corresponding yields decrease fast. Secondly, with an increase of the neutron number in the light isotopes of H, He and Li, the differences between the yields calculated with F15 and Fa3 enlarge (diminish) for symmetric (asymmetric) isotopes, while for the heavier Be, B, and C elements the isotope distributions are almost the same for F15 and Fa3. This can be understood based on the density dependence of the symmetry potentials shown in Fig. 1: for He and Li isotopes, a weak enhancement of isospin symmetric isotopes with Fa3 is shown but this is not observed for neutron rich isotopes. This is because the n/p ratio for free nucleons, as calculated with Fa3, is much larger than that with F15, which leads to the reduction of the N/Z ratios for H, He, and Li when calculated with Fa3.

The light charged particles like triton and ^{3}He ought to be particularly noted, because they

exhibit a considerable difference in the isospin asymmetry, as well as large yields in heavy ion collisions at SIS energy, $E_b \lesssim 1A$ GeV. Both the FOPI [23] and the EOS [24] collaborations have found that - in central Au+Au collisions - ^{3}He clusters have a systematically larger mean kinetic energy than tritons up to bombarding energies of $400A$ MeV. This trend is also found in our calculations. Fig. 6 shows the yield of tritons is larger than that of ^{3}He. To see the symmetry potential effect more clearly, Fig. 7 shows the $t/^3$He ratios as calculated with the four different forms of the symmetry potential used in this work. The dashed line is for the case with the rapidity cut and the solid line is for the case without any kinematical cut. Fig. 7 shows that the $t/^3$He ratios are more strongly enhanced with a softer symmetry potential at mid-rapidity $|y_c^{(0)}| < 0.5$ than without any cut. This is because neutron-richer matter is formed in the mid-rapidity region with an increasingly softer symmetry potential. Thus, more (less) tritons (^{3}He) are produced with a softer symmetry potential as compared to the case without any cut. The magnitudes of the calculated $t/^3$He ratios can be ordered as follows: $X_{DDH\rho^*} > X_{DDH3\rho\delta^*} > X_{Fa3} > X_{F15}$. This is a little different from the ordering of the π^-/π^+ ratios. However, the difference of $t/^3$He is very small between Fa3 and DDH3$\rho\delta^*$. D_{max} is about 22% for the $t/^3$He ratio in full phase space (4π) and $D_{max} \simeq 27\%$ for the $|(y_c^{(0)}| < 0.5$ case. This is larger than in the case of pions as given in Tables I and II. Comparing with Fig. 1 it becomes clear that the ordering of the $t/^3$He ratios for the four different forms of the symmetry potential corresponds to the ordering of the $E_{\rm sym}^{pot}$ at subnormal densities! This holds, regardless of the behavior at $u > 1$. Therefore, we consider the $t/^3$He ratio as a sensitive probe of the density dependence of the symmetry potential at subnormal densities.

In summary, we have investigated the influence of different density dependences of the symmetry potential on charged pion yields, the π^-/π^+ ratio, the n/p ratio for free nucleons, the isotope distribution of H, He, Li, Be, B, C and the $t/^3$He ratio for $^{208}Pb +^{208} Pb$ ($\delta \simeq 0.212$), $^{132}Sn +^{124} Sn$ ($\delta \simeq 0.218$), and $^{96}Zr +^{96} Zr$ ($\delta \simeq 0.167$) at $E_b = 0.4A$ GeV, respectively. We have shown that the negatively charged pion yields, and the π^-/π^+ ratios at low momenta are very sensitive to the density dependence of the symmetry potential at high densities, while the n/p ratio, i.e., for free nucleons, and the $t/^3$He ratio are sensitive to the potential at subnormal densities. The n/p ratios at high transverse momenta show sensitivity to the behavior of the symmetry potential at high densities. To obtain the full information on the density dependence of the symmetry potential, several sensitive probes

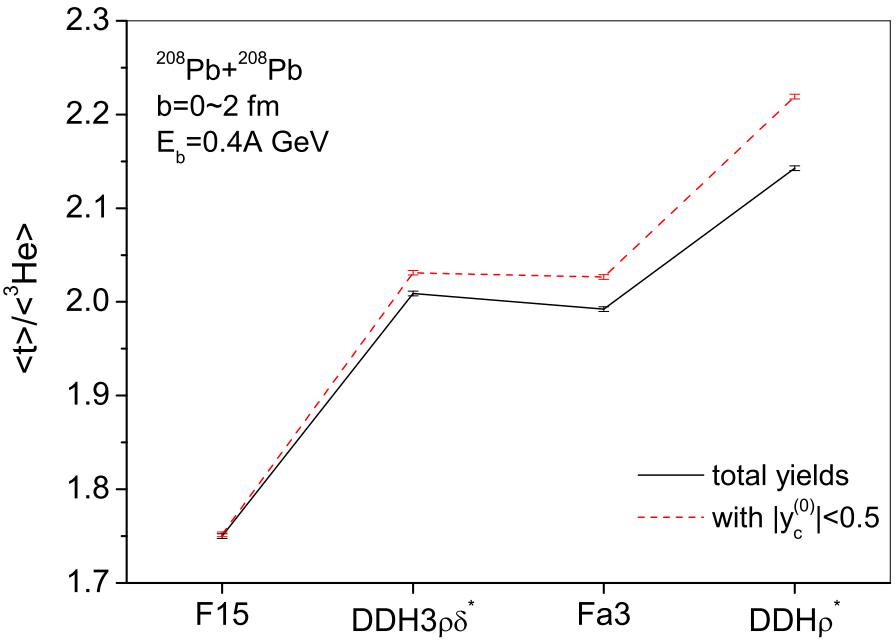

FIG. 7: The ratios of the triton and ^{3}He yields with and without rapidity cut as calculated with four different forms of symmetry potentials.

at both high and low densities were analyzed simultaneously. The comparison of the results of different systems shows that it is suitable to use stable but highly isospin-asymmetric systems to study the effects of different symmetry potentials.

Here, it should be mentioned again that concrete values for the yields of emitted pions, neutrons, protons, tritons, and ^{3}He may be influenced by the uncertainty of the isospin-independent (and the momentum dependent) part of the EoS. However, we expect that the dependence of the n/p , π^-/π^+, and $t/^3$He ratios on the symmetry potential is not strongly affected.

Acknowledgments

Q. Li thanks the Alexander von Humboldt-Stiftung for a fellowship. This work is partly supported by the National Natural Science Foundation of China under Grant No. 10255030,

by GSI, BMBF, DFG, and VolkswagenStiftung.

---

[1] I. Bombaci and U. Lombardo, Phys. Rev. C **44**, 1892 (1991).

[2] B. A. Brown, Phys. Rev. Lett. **85**, 5296 (2000).

[3] T. Gaitanos *et al.*, Nucl. Phys. A. **732**, 24 (2004).

[4] FOPI Collaboration, Z. G. Xiao *et al.*, submitted to Nucl. Phys. A.

[5] Q. Li, Z. Li, E. Zhao, and Raj K. Gupta, Phys. Rev. C **71**, 054907 (2005).

[6] D. Vretenar, T. Niksic, and P. Ring, Phys. Rev. C **68**, 024310 (2003).

[7] E. N. E. van Dalen, C. Fuchs, and Amand Faessler, Nucl. Phys. A **744** 227 (2004).

[8] S. A. Bass *et al.*, Prog. Part. Nucl. Phys. **41**, 225 (1998).

[9] M. Bleicher *et al.*, J. Phys. G: Nucl. Part. Phys. **25**, 1859 (1999).

[10] H. Weber, E. L. Bratkovskaya, W. Cassing, and H. Stöcker, Phys. Rev. C **67**, 014904 (2003).

[11] E. L. Bratkovskaya, M. Bleicher, M. Reiter, S. Soff, H. Stöcker, M. van Leeuwen, S. A. Bass, W. Cassing, Phys. Rev. C **69**, 054907 (2004).

[12] J. Rizzo, M. Colonna, M. Di Toro, and V. Greco, Nucl. Phys. A **732**, 202 (2004).

[13] B.-A. Li, C. B. Das, S. D. Gupta, and C. Gale, Nucl. Phys. A **735**, 563 (2004).

[14] B.-A. Li, G.-C Yong, and W. Zuo, Phys. Rev. C **71**, 014608 (2005).

[15] Q. Li, Z. Li, S. Soff, M. Bleicher, H. Stöcker, to be submitted.

[16] M. B. Tsang *et al.*, Phys. Rev. Lett. **86**, 5023 (2001); *ibid*, **92**, 062701 (2004).

[17] Y. Zhang and Z. Li, Phys. Rev. C **71**, 024604 (2005).

[18] H. Kruse, B.V. Jacak, J.J. Molitoris, G.D. Westfall, H. Stöcker, Phys. Rev. C **31**, 1770 (1985).

[19] W. Neubert and A. S. Botvina, Eur. Phys. J. A **7**, 101 (2000); *ibid*, **17**, 559 (2003).

[20] S. A. Bass, C. Hartnack, H. Stöcker, and W. Greiner, Phys. Rev. C **50**, 2167 (1994).

[21] Q. Li and Z. Li, Phys. Rev. C **64**, 064612 (2001).

[22] L.-W. Chen, C. M. Ko, and B.-A. Li, Phys. Rev. C **68**, 017601 (2003); *ibid*, **69**, 054606 (2004).

[23] FOPI Collaboration, G. Poggi *et al.*, Nucl. Phys. A **586**, 755 (1995).

[24] EOS Collaboration, M. Lisa *et al.*, Phys. Rev. Lett. **75**, 2662 (1995).